Published in final edited form as:
J Am Chem Soc. 2005 December 7; 127(48): 16882–16891. doi:10.1021/ja053800o.

SPECTROSCOPIC STUDIES OF THE ANAEROBIC ENZYME-SUBSTRATE COMPLEX OF CATECHOL 1,2-DIOXYGENASE

Geoff P. Horsman[1], **Andrew Jirasek**[2,3,†], **Frédéric H. Vaillancourt**[1,†], **Christopher J. Barbosa**[2,3,†], **Andrzej A. Jarzecki**[4,†], **Changliang Xu**[4], **Yasmina Mekmouche**[5,†], **Thomas G. Spiro**[4], **John D. Lipscomb**[5], **Michael W. Blades**[2], **Robin F.B. Turner**[3,6], and **Lindsay D. Eltis**[1,**]

[1]Departments of Biochemistry and Microbiology, The University of British Columbia, Vancouver, BC, V6T 1Z3, Canada

[2]Department of Chemistry, The University of British Columbia, Vancouver, BC, V6T 1Z1, Canada

[3]Michael Smith Laboratories, The University of British Columbia, Vancouver, BC, V6T 1Z4, Canada

[4]Department of Chemistry, Princeton University, Princeton, NJ, 08544, USA

[5]Department of Biochemistry, Molecular Biology and Biophysics, University of Minnesota, Minneapolis, MN, 55455, USA

[6]Department of Electrical and Computer Engineering, The University of British Columbia, Vancouver, BC, V6T 1Z4, Canada

Abstract

The basis of the respective regiospecificities of intradiol and extradiol dioxygenase is poorly understood and may be linked to the protonation state of the bidentate-bound catechol in the enzyme:substrate complex. Previous ultraviolet resonance Raman (UVRR) and UV-visible (UV-vis) difference spectroscopic studies demonstrated that in extradiol dioxygenases, the catechol is bound to the Fe(II) as a monoanion. In this study, we use the same approaches to demonstrate that in catechol 1,2-dioxygenase (C12O), an intradiol enzyme, the catechol binds to the Fe(III) as a dianion. Specifically, features at 290 nm and 1550 cm^{-1} in the UV-vis and UVRR difference spectra, respectively, are assigned to dianionic catechol based on spectra of the model compound, ferric tris(catecholate). The UVRR spectroscopic band assignments are corroborated by density functional theory (DFT) calculations. In addition, negative features at 240 nm in UV-vis difference spectra and at 1600, 1210, and 1175 cm^{-1} in UVRR difference spectra match those of a tyrosinate model compound, consistent with protonation of the axial tyrosinate ligand when it is displaced from the ferric ion coordination sphere upon substrate binding. The DFT calculations ascribe the asymmetry of the bound dianionic substrate to the trans donor effect of an equatorially ligated tyrosinate ligand. In addition, the computations suggest that trans donation from the tyrosinate ligand may facilitate charge-transfer from the substrate to yield the iron-bound semiquinone transition state, which is capable of reacting with dioxygen. In illustrating the importance of ligand trans effects in a biological system, the current study demonstrates the power of combining difference UVRR and optical spectroscopies to probe metal ligation in solution.

**Corresponding author: Lindsay D. Eltis, leltis@interchange.ubc.ca.
†Present addresses: AJ: Dept. of Physics and Astronomy, The University of Victoria, Victoria, BC, V8W 3P6, Canada; FHV: Dept. of Biological Chemistry and Molecular Pharmacology, Harvard Medical School, Boston, MA, 02115, USA; CJB: Inex Pharmaceuticals, Burnaby, BC, V5J 5J8, Canada; AAJ: Department of Chemistry, Brooklyn College and the Graduate School of the City University of New York, Brooklyn, NY, 11230, USA; YM: Faculté des Sciences de Saint Jérôme, case 432, Avenue Escadrille Normandie-Niemen, 13397 Marseille Cedex 20, France

INTRODUCTION

Microorganisms are responsible for the bulk of the degradation of aromatic compounds in the biosphere. The aerobic degradation of these compounds typically proceeds via a catecholic intermediate that is cleaved with the incorporation of molecular oxygen into the product. The ring-cleavage reactions are catalyzed by one of two classes of dioxygenases, distinguished on the basis of regiospecificity: the intradiol dioxygenases use non-heme Fe(III) to cleave the carbon-carbon bond of the enediol, while extradiol dioxygenases generally use non-heme Fe(II) to cleave the bond adjacent to the enediol (Scheme 1). Although much has been learned about each enzyme class and the reactions they catalyze, the origins of their respective regiospecificities are not completely understood (for reviews see[1–4]).

Despite the very different active sites of intradiol and extradiol dioxygenases, it has been proposed that the respective catalytic mechanisms proceed via similar bridged iron-alkylperoxo intermediates. In extradiol dioxygenases, the ferrous ion is coordinated by two histidines, a glutamate/aspartate, and two solvent species.[5] The catecholic substrate binds in a bidentate manner, displacing the two solvent ligands[6–10] and activating the ferrous ion towards O_2 binding.[1,7,11] An iron-bound superoxide species is proposed to attack the bound catechol to form the above-mentioned bridged intermediate.[8,12] In intradiol dioxygenases, the ferric ion coordination sphere consists of two histidines, two tyrosines, and hydroxide[13] in a trigonal bipyramidal geometry.[14–19] The axial tyrosine and the hydroxide are displaced upon substrate binding (Figure 1).[16,17,20,21] In contrast to what occurs in extradiol enzymes, binding of the catechol is thought to activate the latter towards direct reaction with oxygen.[22–24] The resulting alkyl peroxide would then bind to the iron to form the bridged intermediate.[22,25,26]

In both enzyme classes, the catecholic substrate binds to iron in a bidentate, asymmetric manner (i.e., inequivalent Fe-O bond lengths).[17,20,28] In extradiol dioxygenases, the asymmetry reflects the monoanionic nature of the Fe(II)-bound catechol. A conserved second sphere histidine (His241 in 2,3-dihydroxybiphenyl 1,2-dioxygenase) residue likely assists in substrate deprotonation.[28] The origin of the asymmetry in intradiol dioxygenases is unclear. Visible resonance Raman studies of catechol 1,2-dioxygenase (C12O) showed that the spectrum of the enzyme-substrate complex is similar to the spectra of model compounds containing Fe(III)-bound dianionic catechol, suggesting that the C12O-bound catechol is also dianionic.[29] Dianionic binding is consistent with the increased Lewis acidity of the ferric center. Further, the displacement of tyrosinate and hydroxide by the dianion would maintain charge neutrality at the metal center. In this scenario, the displaced tyrosinate and hydroxide would deprotonate both catecholic hydroxyls.[20] However, the proposed dianionic binding is somewhat contradictory to the inequivalent Fe-O bond lengths observed in crystallographic structures of C12O:catechol complexes. This asymmetry may originate from trans ligand effects; a tyrosinate ligand is opposite the long Fe-O bond, and a histidine is opposite the short Fe-O bond.[17,20] An interaction between a highly conserved arginine residue and the catecholate oxygen of the long Fe-O bond may also be involved in inducing asymmetry.[20] The importance of this arginine residue has been demonstrated by the inability to grow on 4-hydroxybenzoate of an *Acinetobacter* strain containing an Arg457Ser mutant of protocatechuate 3,4-dioxygenase (PCD).[30] Finally, it is possible that the asymmetric binding reflects ketonization of the substrate.

In intradiol dioxygenases, ketonization of the bound catechol has been proposed to occur only in the transition state and to be stabilized by O_2. Thus, the visible RR spectra indicate that the C12O-bound catechol is not significantly ketonized. Spectroscopic studies of substrate analogs bound to PCD provided the initial proposal for iron-activation of substrate

by ketonization.22 The high affinity of PCD for a ketonized analog of protocatechuate, 2-hydroxyisonicotinic acid *N*-oxide (INO), further implicated substrate ketonization as a key feature of the transition state.31 Analysis of the enzyme-analog complex32 showed electronic absorption spectrum resembled the first intermediate formed upon addition of O_2 to the enzyme-substrate complex.25 This led to the hypothesis that O_2 was required to stabilize the ketonized substrate.32 Thus it is expected that the bound substrate is primarily in the dianionic catecholate form, with ketonization occurring in the presence of oxygen. In the absence of direct evidence of a ketonized substrate, the asymmetry of the bound catecholate is rationalized by trans ligand effects and/or the effect of the arginine residue.

Herein, we describe studies employing UV-vis and UV resonance Raman (UVRR) spectroscopies to further investigate the ground state of the anaerobic C12O catechol complex. UVRR spectroscopy has become a valuable tool to study protein dynamics33,34 and enzyme substrate interactions.28,35–39 We have developed a specialized fiber optic UVRR system,40–42 which enables acquisition of high quality spectra in short (10 s) time scales, hence minimizing photodamage to the sample. This system enabled the characterization of catechol binding in an extradiol dioxygenase.28 Difference spectra (enzyme:substrate (ES) - free enzyme (E)) were compared to spectra of four types of species: (i) free catechol in different ionization states; (ii) an Fe(III)-bound dianionic catechol model compound; (iii) an analog of ketonized catechol, 2-hydroxypyridine *N*-oxide (HPNO); and (iv) *N*-acetyl-L-tyrosinamide. Density functional theory (DFT) calculations facilitated the assignment of dianionic catechol UVRR spectroscopic features, and were used to probe the nature of the ES complex. The power of combining these spectroscopic approaches to probe metal ligation in biological systems is discussed.

EXPERIMENTAL SECTION

Chemicals

Catechol, sodium *tert*-butoxide, sodium hydrosulfite, *tert*-butyl alcohol, *N*-acetyl-L-tyrosinamide, and HPNO were purchased from Sigma-Aldrich (Mississauga, ON, Canada). Deuterium oxide, sodium deuterioxide, *tert*-butyl alcohol-OD, and catechol-d_6 were from Cambridge Isotope Laboratories (Andover, MA) or from C/D/N Isotopes (Pointe-Claire, QC, Canada). The potassium salt of the ferric tris(catecholate) complex, $[Fe(Cat^{2-})_3]^{3-}$, was prepared under a nitrogen atmosphere according to the standard procedure,43 and the crystalline solid was stored under nitrogen until needed. The identity of $[Fe(Cat^{2-})_3]^{3-}$ was confirmed from its UV-vis and UVRR spectra (see RESULTS AND ANALYSIS section). For example, a broad electronic absorption band at 490 nm (ε = 4500 M^{-1} cm^{-1}) and a maximum at 290 nm was consistent with literature values.44–47

Preparation of Samples

Aqueous solutions were prepared using water purified on a Barnstead NANOpure UV apparatus to a resistivity greater than 17 MΩcm. Samples for spectroscopy were prepared under an inert atmosphere in a Mbraun Labmaster glovebox (Stratham, NH) maintained at less than 1 ppm O_2. Buffers and solvents were vigorously bubbled with argon for 20 minutes, brought into the glovebox and allowed to equilibrate for 24 hours prior to use. Catechol and catechol-d_6 were weighed in small glass vials (Wheaton, Millville, NJ) and transferred to the glovebox for sample preparation. C12O was purified chromatographically from sodium benzoate-grown cells of *Pseudomonas putida* mt-2 (ATCC 23973, cured of the TOL plasmid)48 and flash frozen in liquid nitrogen for storage as described previously.49 Aliquots of C12O (500 to 700 μL) were transferred to the glovebox, thawed immediately prior to use, and exchanged into 20 mM Tris-Cl, pH 7.5 by gel filtration chromatography using a 1.5 cm × 8 cm column of Biogel P6 DG (Bio-Rad, Mississauga, ON, Canada). The

ES complex was prepared by adding catechol or catechol-d_6 to an appropriate amount of C12O. Samples for UVRR spectroscopy also contained 100 mM Na_2SO_4. Samples for spectroscopy were transferred to appropriate airtight vials and removed from the glovebox. Samples for UVRR spectroscopy were flash frozen in liquid nitrogen upon removal from the glovebox. C12O concentrations (Fe(III)-containing active sites) were determined spectrophotometrically using a molar absorptivity at 440 nm of 4.3 $mM^{-1}cm^{-1}$.49 These values were consistent with protein concentrations determined using the Bradford method50 and knowledge of the iron content from atomic absorption measurements.

UV-vis absorption spectroscopy

Spectra of free compounds were recorded using a Varian Cary 1E spectrophotometer equipped with a thermostatted cuvette holder (Varian Canada, Mississauga, ON, Canada) set at 25 °C, controlled by Cary WinUV software version 2.00. The spectra of C12O, C12O:catechol, and C12O:HPNO were recorded using a Varian Cary 5000 spectrophotometer with a temperature-controlled cuvette holder set at 25 °C. A 1 mL gas-tight cuvette (Hellma, Concord, ON, Canada) was used for anaerobic acquisition of spectra. A conventional 1-mL cuvette was used for activity assays.

Determination of the Dissociation Constant

Aliquots of catechol (~10 μL) at millimolar concentrations were added to a sealed cuvette containing 1 mL of a 20 μM solution of C12O (based on iron-containing active sites) in 20 mM Tris-Cl, pH 7.5. After each catechol addition, the sealed cuvette was removed from the glovebox and the electronic absorption spectrum was recorded. The fraction of catechol bound was determined by the ratio of the change in absorbance at 390 nm relative to the maximum change after addition of a large excess of catechol. The concentration of bound catechol, [ES], was obtained by multiplying this fraction by the total concentration of active sites, $[E]_0$. Free catechol concentration, $[S]_f$, was calculated as the difference between the total catechol concentration and [ES]. Equation 151 was fit to a plot of [ES] versus $[S]_f$ using the LEONORA program52 to yield a value for the dissociation constant, K_D.

$$[ES]=([E]_0[S]_f)/([S]_f+K_D) \quad (1)$$

The recorded UV-vis spectra were also used to verify that no detectable cleavage of the substrate occurred during these experiments; the product, cis,cis-muconate, has an absorption band at 260 nm.

Activity measurements

Enzymatic activity was measured spectrophotometrically by monitoring the appearance of product at 260 nm (ε = 16.9 $mM^{-1}cm^{-1}$).53 Initial velocities were determined from progress curves by analyzing the data using the Cary WinUV software. The activity assay was performed in a total volume of 1.0 mL of airsaturated 50 mM Tris-Cl, pH 7.5, 25.0 ± 0.1°C containing 300 μM catechol. The reaction was initiated by injecting 5 μl of an appropriate dilution of enzyme into the cuvette.

UVRR measurements

The UVRR spectroscopy instrumentation has been described in detail elsewhere.28,40,54,55 Briefly, UV laser light was generated using a frequency doubled Ar^+ laser operating at 248 nm (Innova 90C, FreD, Coherent Inc, Santa Clara, CA). This incident wavelength provided sufficient substrate resonance enhancement while minimizing the sample fluorescence observed at longer incident wavelengths (e.g. 257 nm). Shorter incident wavelengths, such as 238 nm, increased the signal from aromatic amino acid residues. Although 248 nm

selectively enhances the aromatic ring vibrations in the substrate, hydroxyl vibrations that are coupled to the ring vibrations will also be enhanced to a degree. Fiber optic probes designed specifically for UVRR spectroscopy were utilized for both laser light delivery to the sample as well as collection of Raman scattered light.54 The laser power was kept at a constant 10 mW at the sample. Raman scattered light, which passed through the collection fibers, was incident on a 1 m focal length monochromater (model 2061, McPherson Inc, Chelmsford, MA) equipped with a 3600 groove/mm holographic grating. Wavelength-dispersed light was collected with a liquid nitrogen-cooled CCD detector operating at a fixed temperature of −120 °C (Spec-10 400B, Roper Scientific, Trenton, NJ). Data manipulation was performed using Grams32 spectroscopic software (Thermo Galactic Industries, Salem, NH).

Samples were prepared in 110 μL aliquots and housed in plastic microtubes. A custom designed sample spinner was employed to continually spin the samples during the acquisition of data. Flash frozen samples were thawed under argon flow and transferred to the microtubes using an airtight syringe. Microtubes were also kept under argon flow, and hence all samples were kept under anaerobic conditions during the sample preparation, transfer, and data collection stages. Three acquisitions of 10 s each were collected on each sample, ensuring that no individual sample was exposed to more than 30 s of 10 mW laser light. During initial spectroscopic data acquisition on enzyme samples, 10 μL of material was removed after each 10 s acquisition. Activity assays of these aliquots established that the enzyme lost no more than ~20% of its initial activity over the course of 30 s of laser exposure. To further verify sample integrity during the experiment, and to increase the signal-to-noise ratio, successive spectra acquired from a given sample were compared via difference spectroscopy. Spectra were averaged only if no significant changes occurred in the spectra during the UVRR experiment. All spectra were normalized using the 982 cm^{-1} peak of the Na_2SO_4 internal standard prior to calculating difference spectra. Enzyme turnover did not occur as judged by the lack of signal from the product, *cis,cis*-muconic acid, which gives a strong signal at 1640 cm^{-1}.

Computional methods

DFT computations were performed with the Gaussian 98 program package, using the B3LYP gradient-corrected hybrid density functional to optimize structures and calculate vibrational frequencies. This functional combines Becke's three-parameter hybrid of the gradient-corrected exchange (B3)56 and the exact HF (Hartree-Fock) exchange with the Lee, Yang and Parr (LYP)57 gradient-corrected correlation functional. For the basis set functions, we applied the 5-d component set, comprised of the standard 6-31G* basis functions58 on the O and H atoms and Ahlrichs' valence triple-ζ (VTZ) basis set on the Fe atom59.

Computed frequencies for model structures of $Fe(III)Cat^{2-}$ within C_{2v} symmetry and $Fe(III)Cat^{2-}….NH_4^+$ within Cs symmetry are all positive, indicating that these structures are within their true minima. The optimum Cs symmetry structures of extended models, $Fe(III)L_3Cat^{2-}$ and $Fe(III)L_3Cat^{2-}….NH_4^+$, where one phenoxide and two ammonia ligands are added, give 2 imaginary frequencies. These imaginary frequencies indicate rotation of the phenyl group and asymmetric rotation of NH_3. The effects of these rotations on high frequency modes of the catecholate ligand are expected to be negligible.

We also evaluated selected excited states of the Fe complexes using the time-dependent density functional approximation (TDDFT)60–62 with B3LYP functional, as implemented in the Gaussian 98 suite of programs.

RESULTS AND ANALYSIS

UV-vis absorption spectroscopy of model compounds

To facilitate interpretation of the spectrum of the ES complex, the spectra of the following compounds were recorded: (i) each of the three ionic forms of catechol (generated in solution using the reported pK_a values of 9.45 and 13.3)63; (ii) $[Fe(Cat^{2-})_3]^{3-}$; (iii) each of the two ionic forms of *N*-acetyl-L-tyrosinamide; and (iv) HPNO. The spectrum of $[Fe(Cat^{2-})_3]^{3-}$ was recorded to investigate how binding to Fe(III) perturbs the spectrum of dianionic catechol. Spectral shifts have been reported in resonance Raman and electronic absorption analysis of $[Fe(Cat^{2-})_3]^{3-}$.47 Spectra of two protonation states of *N*-acetyl-L-tyrosinamide were recorded to investigate the displacement of a tyrosinate ligand that accompanies substrate binding in intradiol dioxygenases.16,17,20,21,64,65 Finally, HPNO may serve as an analog of ketonized catechol.

The electronic absorption spectra of the three ionization states of catechol have been previously described.28 The lowest energy absorption maxima (termed the L_b transition by Platt66) of catechol (275 nm) is red-shifted by deprotonation to the monoanion (289 nm), and further red-shifted upon formation of the dianion (308 nm). This absorption maximum of the dianionic catechol is significantly blue-shifted when bound to Fe(III) in the $[Fe(Cat^{2-})_3]^{3-}$ complex (290 nm) (Figure 2).

Protonated *N*-acetyl-L-tyrosinamide (at pH 7) has a strong transition at 223 nm (ε = 8.7 mM^{-1} cm^{-1}), and a weaker band at 275 nm (ε = 1.5 mM^{-1} cm^{-1}) with a shoulder at 281 nm (ε = 1.2 mM^{-1} cm^{-1}). Deprotonation of the hydroxyl results in a red shift and increased intensities such that the strongest feature occurs at 242 nm (ε = 11.9 mM^{-1} cm^{-1}), and a weaker feature at 292 nm (ε = 2.5 mM^{-1} cm^{-1}). The molar absorptivity of the 242 nm feature agrees with that reported by Asher et al. (11.6 mM^{-1} cm^{-1} in water).67 Since the difference (ES – E) spectrum is used to determine the bound substrate spectrum, the difference spectrum (tyrosine – tyrosinate) of *N*-acetyl-L-tyrosinamide is provided in Figure 2.68

HPNO is an analog of the ketonized tautomer of catechol. Significant keto character (i.e. 1-hydroxypyridine-2-one) is observed in ethanol,69 water,70 DMSO,71 the solid state,71 and the vapor phase.72 Electronic absorption studies have identified unique bands related to each tautomer. For example, HPNO and its derivatives *N*-methoxy- and *N*-benzyloxy-2-pyridone ('locked' in the keto tautomer) have absorption maxima around 300 nm.69,70 When ketonization is made less favorable by making the 2-methoxy- or 2-benzyloxypyridine-*N*-oxide, the 300 nm feature decreases in intensity and the major feature appears at 247–260 nm, which is thought to be related to the 2-hydroxy tautomer.69,70 Studies of the 2-pyridone and 2-hydroxypyridine tautomerization show similar results.73 Consistent with these studies, our spectrum of deprotonated HPNO ($HPNO^-$) does not exhibit a 260 nm feature, indicating primarily the keto form in solution (Figure 2). Further, the spectrum shows an absorbance maximum at 312 nm, only 4 nm red-shifted from the fully deprotonated catechol ($catechol^{2-}$; 308 nm).

UV-vis absorption of C12O-bound catechol

Anaerobic spectra of C12O were recorded before and after titration with catechol. As typically seen for intradiol enzymes,74 the characteristic burgundy-red color of the enzyme disappeared as catechol was added, replaced by a grayish-blue color of the anaerobic ES complex. This was observable in the UV-vis spectrum as a decrease in absorbance in the 350–500 nm region and a corresponding increase in the region above 500 nm, which are considered to arise from loss of tyrosinate-to-iron and gain of catecholate-to-iron charge transfer transitions, respectively.29 These charge-transfer bands provide a simple means by

which to calculate the dissociation constant for catechol (K_D = 1.4 ± 0.2 μM, 20 mM Tris-Cl, pH 7.5, 25 °C). The observed spectral changes and K_D of C120 from *P. putida* mt-2 for catechol are very similar to those seen in C12O from *P. arvilla* C-1 (K_D = 2.1 μM, 50 mM potassium phosphate, pH 7.5, 4 °C;26 ββ isozyme (there are also αα and αβ isozymes) has 98% sequence identity with *P. putida* mt-275).

To determine the spectrum of C12O-bound catechol, the free enzyme (E) spectrum was subtracted from the spectrum of the anaerobic ES complex (Figure 2). The absorbance of the enzyme contributed to high background below 240 nm. At catechol concentrations exceeding that of enzyme, an absorption peak corresponding to free neutral catechol appeared at 275 nm (data not shown). Two major features were apparent in the difference spectrum: a negative peak at or just below 240 nm, and a positive feature consisting of maxima at 290 and 297 nm. A minor feature centered at 345 nm was also observed.

The negative peak at ~240 nm correlates very well to the loss of tyrosinate upon protonation (upon subtraction of tyrosinate in free enzyme from tyrosine in ES complex). The intensity of this peak (ε ~4.3 mM^{-1} cm^{-1}) is less than expected for tyrosinate (ε ~ 12 mM^{-1} cm^{-1}), but this could be explained if we assume that the bound catechol absorbs in this region. Free monoanionic, free dianionic, and Fe(III)-bound dianionic catechols all have similar absorptivities at 240 nm (6 – 7 mM^{-1} cm^{-1}), so subtraction of tyrosinate from a catecholic absorption band could quantitatively account for the intensity of the observed negative feature. Thus the negative tyrosinate feature may be regarded as evidence for protonation of the tyrosinate ligand, consistent with its proposed role as a base.

The major feature of the C12O-bound substrate at 290/297 nm is in reasonable agreement with the 290 nm band of $[Fe(Cat^{2-})_3]^{3-}$. Two factors may contribute to the former's perturbation to 297 nm: (a) the asymmetric bond lengths of the bound catechol and (b) the polarizing effect of a conserved Arg218 (Arg221 in C12O from *Acinetobacter* ADP1, and Arg457 in PCD from *P. putida*). The assignment of the weak band at 345 nm is uncertain, and warrants further investigation.

UV-vis absorption of C12O-bound HPNO

Since HPNO has keto character in solution, the C12O:HPNO complex may provide spectral markers of ketonized catechol in the enzyme active site. Based on the disruption of the tyrosinate-to-iron charge transfer band, HPNO bound quantitatively to C12O such that the K_D could not be reliably determined. Similar complications arising from high affinity were reported for the binding of INO to PCD. In that case, 4-nitrocatechol was used to increase the apparent K_D to a measurable range.32 The disruption of tyrosinate-to-iron charge transfer illustrates that HPNO binds to the ferric site with concomitant tyrosinate displacement, as occurs for catechol. However, the increase in absorbance at >500 nm (catecholate-to-iron charge transfer), which gives a gray-blue color in the C12O:catechol complex, was not observed for C12O:HPNO. Rather, a bleached complex was observed, with spectroscopic features similar to the previously characterized PCD:INO complex.32 Whittaker and Lipsomb observed fluorescence from excitation of this complex at 340 nm, which corresponded to fluorescence from a similar excited state considered to be a marker of ketonization in free INO.32 They thereby concluded that INO bound to PCD with at least some keto character. It is therefore probable that C12O-bound HPNO has some keto character.

The calculated difference spectrum (ES – E; Figure 2) revealed a major peak at 298 nm with a shoulder at 323 and a minor feature at 357 nm. Although the major peak matches the 297 nm feature observed in the C12O:catechol complex, the overall shape of the peak is different. As described below for the UVRR data and DFT calculations, it seems likely that

the long wavelength features in the absorption spectrum of the enzyme-bound catechol are due to the asymmetry of the bound catecholate, and not ketonization of the latter. Curiously, a negative feature at 240 nm was not observed in the difference spectrum of enzyme-bound HPNO. Since the axial tyrosinate of PCD has been shown to dissociate upon HPNO ligation, 20 a negative 240 nm feature such as that seen in the catechol difference spectrum is expected. This discrepancy may originate from the greater signal of bound HPNO in this region, just as some bands of HPNO appear to mask some of the tyrosine bands in the UVRR spectra (see below).

UVRR of model compounds

To interpret features of the UVRR difference spectra, we obtained spectra in both H_2O and D_2O of the model compounds used in the UV-vis experiments. Generally, very small band shifts (<6 cm^{-1}) are observed upon solvent deuteration (Table 1). The major bands are assigned based on comparison to previous studies.[28,76–81] Nevertheless, the difference spectra provide relatively few features. Accordingly, the following discussion focuses on the strongest spectral features of the model compounds.

Figure 3 shows spectra of the monoanionic and dianionic catechol in H_2O, as well as the effects from Fe(III) ($[Fe(Cat^{2-})_3]^{3-}$), ring deuteration (catechol-d_4^{2-}), ketonization ($HPNO^-$), and tyrosinate displacement. Neutral catechol has no strong features in the region of interest (>1500 cm^{-1}) (Table 1). In contrast, mono- and dianionic catechol have a strong 8a band in this region: a strong doublet (1572/1594 cm^{-1}) in the case of the former, and a strong single band at 1553 cm^{-1} in the case of the latter. The 8a band is easily perturbed by catechol ring deuteration (−30 cm^{-1} for $catechol^{2-}$ to catechol-d_4^{2-}), and Fe(III) coordination (+15 cm^{-1} for $catechol^{2-}$ to $[Fe(Cat^{2-})_3]^{3-}$). Although we did not make the corresponding deuterated catechol Fe(III) complex, we can infer that an approximately 15 cm^{-1} upshift would be expected when catechol-d_4^{2-} binds Fe(III), placing the expected band at around 1535 cm^{-1}. The effect of ketonization of catechol (and the resulting asymmetry) was explored using the analog HPNO, which shows strong features at 1542 and 1617 cm^{-1} when fully deprotonated at pH 11. To account for tyrosinate displacement, spectra of both protonation states of *N*-acetyl-L-tyrosinamide were recorded. Tyrosine gives a weak signal at 1616 cm^{-1}, while tyrosinate gives a strong band (~15 times more intense than tyrosine) at 1602 cm^{-1}. Thus we can predict a strong negative feature at around 1600 cm^{-1} in the difference spectrum of bound and unbound enzyme.

UVRR of Enzyme Complexes

The difference spectra of C12O with and without catechol or HPNO have relatively low signal-to-noise (S/N) ratios. In addition, errors accumulate in the spectral subtraction. We therefore estimate the error in the wavenumbers to be about ±2 cm^{-1}. Accordingly, only shifts greater than 4 cm^{-1} were considered. All difference spectra share three major features: a strong negative band at 1600 cm^{-1}; a strong band at 1610–1625 cm^{-1}; and a feature at 1550–1570 cm^{-1}. As discussed below, the intensities and positions of these bands are generally consistent with the most intense features of the model compounds.

The negative feature at 1601 cm^{-1}, as well as the smaller features at ~1175 and 1210 cm^{-1}, match the bands of free tyrosinate with respect to their frequencies and relative intensities (Figure 3g). Accordingly, they are attributed to the subtraction of tyrosinate in free enzyme, consistent with tyrosinate protonation upon catechol ligation. HPNO and catechol produce very similar difference spectra with the exception of the negative tyrosinate features at 1175 and 1210 cm^{-1}, which are absent from the spectrum obtained using HPNO (Figure 4). Nevertheless, the negative 1600 cm^{-1} feature of the difference spectrum obtained with HPNO indicates that the binding of this compound induces tyrosinate protonation, consistent

with previous demonstrations that such *N*-oxide inhibitors cause tyrosinate dissociation in PCD.20 The UVRR spectrum of $HPNO^-$ (Figure 3e) differs from that of catechol (Figure 3a–d) in that it contains strong features around 1180 cm^{-1}. It is likely that these features mask the signal of the expected negative tyrosinate bands in this region of the HPNO difference spectrum.

All difference spectra have a peak at 1550–1570 cm^{-1}, most consistent with a Fe(III)-bound dianionic catechol. With the aid of DFT calculations (see below), we assign this band to catecholate mode 8a, seen at 1568 cm^{-1} in the spectrum of $[Fe(Cat^{2-})_3]^{3-}$. The full-width at half max (FWHM) of the 1550 cm^{-1} feature is ~30 cm^{-1}, consistent with the ~30 cm^{-1} FWHM of the dianion spectrum. In comparison, the monoanion doublet feature has a FWHM of ~50 cm^{-1}. In summary, the position and width of this peak is consistent with dianionic substrate binding. In the catechol difference spectra (Fig. 4a and b), the 8a feature overlaps with the negative 1600 cm^{-1} feature, complicating the reliable assignment of any D_2O-induced shift. Indeed, it is difficult to discern any baseline separation of the 8a and negative 1600 cm^{-1} features. However, a clear downshift of the 8a feature to 1550 cm^{-1} is observed in the catechol-d_6 difference spectrum, which is well separated from the 1600 cm^{-1} band.

Next to the 1601 cm $^{-1}$ negative band is a positive feature at ~1620 cm^{-1}, common to all the spectra. We considered the possibility that this band might arise from the C=O stretch of ketonized catecholate, but the DFT calculations (see below) rule out ketonization in the ground state. (The calculations also indicate similar frequencies for bound $HPNO^-$ as for bound $catechol^{2-}$, despite the former having an authentic C=O bond.) The ~1620 cm^{-1} feature is assigned instead to a signal from the displaced tyrosinate being converted to tyrosine. Tyrosine has its strongest band (Y8a) at 1615 cm^{-1}. While tyrosine is less strongly enhanced than tyrosinate with 248 nm excitation (the ratio is ~15-fold in water), the resonance enhancement factors depend on the environment of the chromophore in the protein, and are difficult to predict. The band occurs at the same frequency in all the ES – E spectra, even those of catechol-d_6, for which large deuteration downshifts are expected (see below). Consequently, the tyrosinate/tyrosine conversion can provide a common origin for the 1601/1620 cm^{-1} negative/positive feature seen in all the spectra.

DFT Computations, Ground State

DFT computations were undertaken to assess the structure of C12O-bound catechol, especially with respect to the issue of ketonization. The models used in the computation are illustrated in Figure 5, along with the computed bond distances.

Initially, we examined $[Fe(Cat^{2-})_3]^{3-}$, in order to compare DFT-computed vibrational frequencies with experimental data (Table 2). Previous studies have used a simplified model, with only one $catechol^{2-}$ bound to Fe^0 78,84; we tested this model and found significant differences in vibrational frequencies with respect to the tris-catecholate Fe^{3+} complex. Computed frequencies for $[Fe(Cat^{2-})_3]^{3-}$ are systematically higher than experimental frequencies (Table 2), as is commonly found for DFT frequencies of organic compounds.85 This discrepancy can be reduced with the SQM (scaled quantum mechanical) method, by applying specific empirical scaling factors for each kind of internal coordinate.85,86 When standard values of these factors85,86 were introduced for $[Fe(Cat^{2-})_3]^{3-}$, agreement with experiment was markedly improved (Table 2), although the highest frequency mode, 8a, was now ~20 cm^{-1} too low. Isotope shifts for C-H(D) exchange were in reasonable agreement with reported values for catechol,78 and with the 33 cm^{-1} downshift between $catechol^{2-}$ and $catechol\text{-}d_6^{2-}$ for the highest frequency UVRR band (mode 8a) (Figure 3).

To model C12O-bound catechol^{2-}, we first replaced two of the catecholates in $[Fe(Cat^{2-})_3]^{3-}$ with three NH_3 molecules, in order to achieve a pentacoordinate complex, with three N ligands. The optimized geometry of this complex was essentially square pyramidal, with two O and two N atoms in roughly the same plane. The Fe-O bonds are equivalent. The computed frequencies for the bound catechol^{2-} (Table 2) increased systematically from those of $[Fe(Cat^{2-})_3]^{3-}$, no doubt a reflection of increased charge donation to the Fe^{3+}, when the competing catechol^{2-} ligands are replaced. Interestingly, the order of the 8a and 8b modes is reversed, with 8b now lying higher (1621 vs 1570 cm^{-1}). This reversal is associated with C-C bond length changes. Relative to $[Fe(Cat^{2-})_3]^{3-}$, the outermost catecholate C-C bond lengthens, by 0.04 Å, while the adjacent bonds shorten by the same amount. These changes correspond with a decrease in the frequency of the 8a mode, whose eigenvector (not shown) mainly involves stretching of the outermost bond, while increasing the frequency of the 8b mode, which primarily involves the adjacent bonds.

Next we replaced one of the ammonia ligands with phenoxide, modeling bound tyrosinate. The geometry now optimized to trigonal bipyramidal, the three O atoms being coplanar with the Fe (Figure 5C). The Fe-O distances reveal pronounced asymmetry, the bond cis to the phenoxide shortening by 0.11 Å. However, the catecholate C-O bonds are equal in length; there is no evidence for catecholate ketonization associated with the Fe-O bonding asymmetry. The vibrational eigenvectors follow the same pattern as in $[Fe(Cat^{2-})_3]^{3-}$, although the vibrational frequencies (Table 2) are somewhat altered. Most of the frequencies decrease (Table 2), reflecting diminished charge transfer from catecholate to Fe^{3+} because of stronger donor competiton from phenoxide than ammonia. However, the mode 8a and 8b frequencies are elevated, to 1601 and 1630 cm^{-1}, because of contributions from the bonds adjacent to the catecholate O atoms, which contract slightly, reflecting increased bond strength.

Finally, to probe the effect of the arginine residue that is H-bonded to the catecholate O atom trans to the tyrosinate ligand, we placed an ammonium ion at the crystallographically-determined distance of 2.5Å; a distance which was kept constant during the optimization. With this constraint, the geometry optimized with the ammonium ion in the FeO_3 plane. By contrast, the arginine H-bond is out of the plane in the C12O crystal structure. However, the influence of this parameter on the rest of the structure is likely to be minimal. The effect was to increase the Fe-O asymmetry further by lengthening the Fe-O bond trans to the tyrosinate. The disparity in the Fe-O distances, 2.08 and 1.86 Å, is similar to that seen in the C12O crystal structure. The catecholate C-O distances are now slightly asymmetric (1.34 and 1.36 Å), but the difference is too small to suggest ketonization. The vibrational frequencies are altered only slightly by inclusion of the ammonium ion: modes 8a and 8b are now at 1613 and 1633 cm^{-1}.

We have not introduced force constant scaling to the enzyme models, because of complexities associated with non-catecholate coordinates. However, it is reasonable to expect that mode 8a is calculated ~30 cm^{-1} too high, as it is for $[Fe(Cat^{2-})_3]^{3-}$ (Table 2). Using the computed frequency for the ammonium ion model, we therefore expect mode 8a to be at ~1580 cm^{-1} for C12O-bound catecholate. ES – E difference Raman spectra (Figure 4) show a positive band near 1570 cm^{-1}, but this band may be distorted by the large negative 1601 cm^{-1} due to the displaced tyrosinate. Significantly, the ES – E spectra of catechol-d_6 show a prominent positive band at 1551 cm^{-1}. Ring deuteration is expected to shift mode 8a down by 35 cm^{-1} (Table 2). Consequently the expected position for undeuterated catecholate is 1586 cm^{-1}, very close to the DFT prediction.

The predicted position for mode 8b is 20 cm^{-1} higher, ~1606 cm^{-1}, a position that is obscured by the negative band of displaced tyrosinate. In any event, the 8b intensity is

probably low. (The mode is not observed at all for $[Fe(Cat^{2-})_3]^{3-}$, Figure 3, because it is antisymmetric with respect to the catecholate C_2 axis, and is not subject to resonance enhancement via the dominant Franck-Condon mechanism. This restriction is relaxed somewhat by the asymmetry resulting from the tyrosinate coordination and arginine H-bonding, but the induced intensity is likely to be small.) Judging from the $[Fe(Cat^{2-})_3]^{3-}$ spectrum (Figure 3), the Raman spectrum is dominated by mode 8a, and other bands are probably lost in the noise of the ES – E spectra.

To explore the issue of ketonization further, we carried out preliminary calculations on the analog of ketonized catecholate, 2-hydroxypyridine *N*-oxide anion, $HPNO^-$. The optimized structure does have a C=O bond (1.24 Å), and a C=O stretching vibration computed at 1734 cm^{-1}. However, chelation of $HPNO^-$ to Fe^{3+} lengthens the C=O bond (1.26 Å), and lowers its force constant so that the C=O coordinate becomes mixed with C-C coordinates in modes with frequencies near 1600 cm^{-1}, the region of the catecholate 8a and 8b modes. Thus it is not surprising that bound C12O-bound $HPNO^-$ is not readily distinguishable from bound catecholate in the ES – E UVRR spectra (Figure 4).

DFT Computations, Excited States

Since no evidence for catecholate ketonization in the ground state can be obtained in the calculations, the possibility of an excited state involving catechol-Fe electron transfer was explored. Evidence from model compound studies supported the catalytic relevance of the resulting Fe(II)-semiquinone,[23,24] which can directly react with oxygen. Time-dependent DFT was used to calculate the low-lying excited states for the $Fe(III)(NH_3)_2(PhO^-)Cat^{2-}$ model. The first three excited states all involve charge transfer to Fe(III) from catechol **π** orbitals (Figure 6). Of particular interest is the LUMO+2, the acceptor orbital for the second excited state (bottom right panel of Figure 6). It shows a clear inequivalence in the catecholate C-O bonds. There is buildup of electron density on the C-O opposite the phenoxide, suggestive of a C=O double bond. In addition, there is excess electron density on the C atom adjacent to the C=O; this is where the incoming O_2 molecule attacks the catecholate ring. The TDDFT-computed excitation energies (see Figure 6 caption) are unlikely to be reliable, but the computations point to LUMO+2 as a conduit to a relatively low-energy charge-transfer state that has the right characteristics for the expected transition state of the enzyme.

Further, the asymmetry of the structure implicates the phenoxide, which, being a strong donor, localizes electron density on the opposite C-O (quasi- C=O) bond, and promotes charge transfer from the adjacent C atom. The same computation with the ammonium added (Figure 5D) produced higher energies, indicating that the positive charge stabilizes the ground state more than the excited state. However this effect may result from improper orientation of the ammonium ion, as the conserved Arg218 (Arg221 in C12O from *Acinetobacter* sp. ADP1, Figure 1) probably plays a catalytic role by stabilizing negative charge. When the excited states were computed for the complex without phenoxide, $Fe(III)(NH_3)_3Cat^{2-}$, there was no tendency toward ketonization, nor any orbital asymmetry. In summary, these calculations implicate the trans tyrosinate ligand as a strong electron donor responsible for inducing asymmetry in the bound catechol, corroborating a conclusion reached by computational and spectroscopic analysis of the substrate-free active site of PCD.[87] Our calculations further implicate a role for the trans tyrosinate in directing the reaction via charge-transfer to an transition state that has Fe(II)-semiquinone character.

CONCLUSIONS

This study describes the direct observation of dianionic catechol bound to C12O and protonation of an endogenous tyrosinate ligand after it dissociates from the ferric center

upon substrate binding. Difference UVRR band assignments were supported by DFT calculations. These calculations implicate the trans tyrosinate ligand as a strong electron donor responsible for inducing asymmetry in the bound catechol, and likely directing the reaction via charge-transfer in the transition state. By contrast, difference UVRR spectroscopy has been used to show that in extradiol dioxygenases, the asymmetry in the bound catechol is induced by mono-deprotonation of the Fe(II)-bound catechol.28 Combining difference UVRR and optical spectroscopies is likely to provide other important insights into metal ligation in solution.

Supplementary Material

Refer to Web version on PubMed Central for supplementary material.

Acknowledgments

This work was supported in part by grants from the Natural Sciences and Engineering Research Council of Canada (NSERC) to L.D.E., the Canada Foundation for Innovation (CFI), the British Columbia Health Research Foundation (BCHRF), and the National Institutes of Health (GM24689) to J.D.L.

REFERENCES

1. Bugg TDH, Lin G. Chem. Commun. 2001:941–952.
2. Costas M, Mehn MP, Jensen MP, Que L. Chem. Rev. 2004; 104:939–986. [PubMed: 14871146]
3. Bugg TDH. Tetrahedron. 2003; 59:7075–7101.
4. Solomon EI, Brunold TC, Davis MI, Kemsley JN, Lee SK, Lehnert N, Neese F, Skulan AJ, Yang YS, Zhou J. Chem. Rev. 2000; 100:235–349. [PubMed: 11749238]
5. Han S, Eltis LD, Timmis KN, Muchmore SW, Bolin JT. Science. 1995; 270:976–980. [PubMed: 7481800]
6. Mabrouk PA, Orville AM, Lipscomb JD, Solomon EI. J. Am. Chem. Soc. 1991; 113:4053–4061.
7. Arciero DM, Orville AM, Lipscomb JD. J. Biol. Chem. 1985; 260:14035–14044. [PubMed: 2997190]
8. Arciero DM, Lipscomb JD. J. Biol. Chem. 1986; 261:2170–2178. [PubMed: 3003098]
9. Vaillancourt FH, Han S, Fortin PD, Bolin JT, Eltis LD. J. Biol. Chem. 1998; 273:34887–34895. [PubMed: 9857017]
10. Sato N, Uragami Y, Nishizaki T, Takahashi Y, Sazaki G, Sugimoto K, Nonaka T, Masai E, Fukuda M, Senda T. J. Mol. Biol. 2002; 321:621–636. [PubMed: 12206778]
11. Davis MI, Wasinger EC, Decker A, Pau MYM, Vaillancourt FH, Bolin JT, Eltis LD, Hedman B, Hodgson KO, Solomon EI. J. Am. Chem. Soc. 2003; 125:11214–11227. [PubMed: 16220940]
12. Winfield CJ, Al-Mahrizy Z, Gravestock M, Bugg TDH. J. Chem. Soc., Perkin Trans. 1. 2000:3277–3289.
13. True AE, Orville AM, Pearce LL, Lipscomb JD, Que L. Biochemistry. 1990; 29:10847–10854. [PubMed: 2271684]
14. Ohlendorf DH, Lipscomb JD, Weber PC. Nature. 1988; 336:403–405. [PubMed: 3194022]
15. Ohlendorf DH, Orville AM, Lipscomb JD. J. Mol. Biol. 1994; 244:586–608. [PubMed: 7990141]
16. Vetting MW, D'Argenio DA, Ornston LN, Ohlendorf DH. Biochemistry. 2000; 39:7943–7955. [PubMed: 10891075]
17. Vetting MW, Ohlendorf DH. Structure. 2000; 8:429–440. [PubMed: 10801478]
18. Ferraroni M, Seifert J, Travkin VM, Thiel M, Kaschabek S, Scozzafava A, Golovleva L, Schlömann M, Briganti F. J. Biol. Chem. 2005; 280:21144–21154. [PubMed: 15772073]
19. Ferraroni M, Solyanikova IP, Kolomytseva MP, Scozzafava A, Golovleva L, Briganti F. J. Biol. Chem. 2004; 279:27646–27655. [PubMed: 15060064]
20. Orville AM, Lipscomb JD, Ohlendorf DH. Biochemistry. 1997; 36:10052–10066. [PubMed: 9254600]

21. Elgren TE, Orville AM, Kelly KA, Lipscomb JD, Ohlendorf DH, Que L. Biochemistry. 1997; 36:11504–11513. [PubMed: 9298971]
22. Que L, Lipscomb JD, Münck E, Wood JM. Biochim. Biophys. Acta. 1977; 485:60–74. [PubMed: 199266]
23. Cox DD, Que L. J. Am. Chem. Soc. 1988; 110:8085–8092.
24. Jang HG, Cox DD, Que L. J. Am. Chem. Soc. 1991; 113:9200–9204.
25. Bull C, Ballou DP, Otsuka S. J. Biol. Chem. 1981; 256:12681–12686. [PubMed: 7309730]
26. Walsh TA, Ballou DP, Mayer R, Que L Jr. J. Biol. Chem. 1983; 258:14422–14427. [PubMed: 6643492]
27. Humphrey W, Dalke A, Schulten K. J. Molec. Graphics. 1996; 14:33–38.
28. Vaillancourt FH, Barbosa CJ, Spiro TG, Bolin JT, Blades MW, Turner RFB, Eltis LD. J. Am. Chem. Soc. 2002; 124:2485–2496. [PubMed: 11890797]
29. Que L, Heistand RH. J. Am. Chem. Soc. 1979; 101:2219–2221.
30. Gerischer U, Ornston LN. J. Bacteriol. 1995; 177:1336–1347. [PubMed: 7868609]
31. May SW, Oldham CD, Mueller PW, Padgette SR, Sowell AL. J. Biol. Chem. 1982; 257:12746–12751. [PubMed: 6813328]
32. Whittaker JW, Lipscomb JD. Journal of Biological Chemistry. 1984; 259:4476–4486. [PubMed: 6323475]
33. Hu XH, Rodgers KR, Mukerji I, Spiro TG. Biochemistry. 1999; 38:3462–3467. [PubMed: 10090732]
34. Lednev IK, Karnoup AS, Sparrow MC, Asher SA. J. Am. Chem.Soc. 1999; 121:4076–4077.
35. Austin JC, Kuliopulos A, Mildvan AS, Spiro TG. Protein Sci. 1992; 1:259–270. [PubMed: 1339027]
36. Austin JC, Zhao QJ, Jordan T, Talalay P, Mildvan AS, Spiro TG. Biochemistry. 1995; 34:4441–4447. [PubMed: 7703258]
37. Couling VW, Fischer P, Klenerman D, Huber W. Biophys. J. 1998; 75:1097–1106. [PubMed: 9675211]
38. Efremov RG, Feofanov AV, Dzhandzhugazyan KN, Modyanov NN, Nabiev IR. FEBS Lett. 1990; 260:257–260. [PubMed: 2153587]
39. Wilson KJ, Mcnamee MG, Peticolas WL. J. Biomol. Struct. Dyn. 1991; 9:489–509. [PubMed: 1726137]
40. Barbosa CJ, Vaillancourt FH, Eltis LD, Blades MW, Turner RFB. J. Raman Spectrosc. 2002; 33:503–510.
41. Schulze HG, Greek LS, Barbosa CJ, Blades MW, Gorzalka BB, Turner RFB. J. Neurosci. Meth. 1999; 92:15–24.
42. Jirasek A, Horsman GP, Vaillancourt FH, Barbosa CJ, Eltis LD, Blades MW, Turner RFB. Am. Pharm. Rev. 2004; 7:49–53.
43. Karpishin TB, Gebhard MS, Solomon EI, Raymond KN. J. Am.Chem. Soc. 1991; 113:2977–2984.
44. Anderson BF, Buckingham DA, Robertson GB, Webb J, Murray KS, Clark PE. Nature. 1976; 262:722–724. [PubMed: 134287]
45. Avdeef A, Sofen SR, Bregante TL, Raymond KN. J. Am. Chem Soc. 1978; 100:5362–5370.
46. Hider RC, Mohdnor AR, Silver J, Morrison IEG, Rees LVC. J. Chem. Soc., Dalton Trans. 1981:609–622.
47. Salama S, Stong JD, Neilands JB, Spiro TG. Biochemistry. 1978; 17:3781–3785. [PubMed: 151556]
48. Wolfe MD, Altier DJ, Stubna A, Popescu CV, Münck E, Lipscomb JD. Biochemistry. 2002; 41:9611–9626. [PubMed: 12135383]
49. Nakai C, Nakazawa T, Nozaki M. Arch. Biochem. Biophys. 1988; 267:701–713. [PubMed: 3214177]
50. Bradford MM. Anal. Biochem. 1976; 72:248–254. [PubMed: 942051]
51. Fersht, A. A. Structure and mechanism in protein science: a guide to enzyme catalysis and protein folding. New York: W. H. Freeman; 1999.

52. Cornish-Bowden, A. Analysis of Enzyme Kinetic Data. New York: Oxford University Press; 1995.
53. Sistrom WR, Stanier RY. J. Biol. Chem. 1954; 210:821–836. [PubMed: 13211620]
54. Greek LS, Schulze HG, Blades MW, Haynes CS, Klein KF, Turner RFB. Appl. Opt. 1998; 37:170–180. [PubMed: 18268575]
55. Greek LS, Schulze HG, Haynes CA, Blades MW, Turner RFB. Appl. Opt. 1996; 35:4086–4095. [PubMed: 21102813]
56. Becke AD. J. Chem. Phys. 1993; 98:1372–1377.
57. Lee CT, Yang WT, Parr RG. Phys. Rev. B. 1988; 37:785–789.
58. Hehre WJ, Ditchfie R, Pople JA. J. Chem. Phys. 1972; 56 2257–&.
59. Schafer, a; Horn, H.; Ahlrichs, R. J. Chem. Phys. 1992; 97:2571–2577.
60. Bauernschmitt R, Ahlrichs R. Chem. Phys. Lett. 1996; 256:454–464.
61. Casida ME, Jamorski C, Casida KC, Salahub DR. J. Chem. Phys. 1998; 108:4439–4449.
62. Stratmann RE, Scuseria GE, Frisch MJ. J. Chem. Phys. 1998; 109:8218–8224.
63. Smith, RM.; Martell, AE. Critical stability constants (second supplement and earlier volumes. New York: Plenum Press; 1989.
64. Briganti F, Mangani S, Pedocchi L, Scozzafava A, Golovleva LA, Jadan AP, Solyanikova IP. FEBS Lett. 1998; 433:58–62. [PubMed: 9738933]
65. Frazee RW, Orville AM, Dolbeare KB, Yu H, Ohlendorf DH, Lipscomb JD. Biochemistry. 1998; 37:2131–2144. [PubMed: 9485360]
66. Platt JR. J. Chem. Phys. 1949; 17:484–495.
67. Asher SA, Larkin PJ, Teraoka J. Biochemistry. 1991; 30:5944–5954. [PubMed: 2043634]
68. In the free enzyme, tyrosinate is coordinated to iron, while in the ES complex, the presumably protonated tyrosine is dissociated from iron. Thus the ES-E spectrum will show negative features from tyrosinate (and weak positive tyrosine features).
69. Shaw E. J. Am. Chem. Soc. 1949; 71:67–70. [PubMed: 18108944]
70. Gardner JN, Katritzky AR. J. Chem. Soc. 1957; 1957:4375–4385. 1957,
71. Ballesteros P, Claramunt RM, Canada T, Focesfoces C, Cano FH, Elguero J, Fruchier A. J. Chem. Soc., Perkin Trans. 2. 1990; 2:1215–1219.
72. La Manna G, Biondi F. J. Mol. Struct. 1993; 106:127–129.
73. Beak P. Acc. Chem. Res. 1977; 10:186–192.
74. Kojima Y, Fujisawa H, Nakazawa A, Nakazawa T, Kanetsun F, Taniuchi H, Nozaki M, Hayaishi O. J. Biol. Chem. 1967; 242:3270–3278. [PubMed: 6029438]
75. Nakai C, Uyeyama H, Kagamiyama H, Nakazawa T, Inouye S, Kishi F, Nakazawa A, Nozaki M. Arch. Biochem. Biophys. 1995; 321:353–362. [PubMed: 7646060]
76. Almenningen A, Bastiansen O, Fernholt L, Cyvin BN, Cyvin SJ, Samdal S. J. Mol. Struct. 1985; 128:59–76.
77. Greaves SJ, Griffith WP. Spectrochim Acta, Part A. 1991; 47:133–140.
78. Ohrstrom L, Michaud-Soret I. J. Phys. Chem. A. 1999; 103:256–264.
79. Ramirez FJ, Lopez-Navarrete JT. Vib. Spectrosc. 1993; 4:321–334.
80. Zerbi G, Sandroni S. Spectrochim. Acta, Part A. 1968; A 24:483–510.
81. Zerbi G, Sandroni S. Spectrochim. Acta, Part A. 1968; A 24:511–528.
82. Copeland RA, Spiro TG. Biochemistry. 1985; 24:4960–4968. [PubMed: 3000420]
83. Koh TY, Greaves SJ, Griffith WP. Spectrochim. Acta, Part A. 1994; 50:857–873.
84. Ohrstrom L, Michaud-Soret I. J. Am. Chem. Soc. 1996; 118:3283–3284.
85. Rauhut G, Pulay P. J. Am. Chem. Soc. 1995; 117:4167–4172.
86. Rauhut G, Jarzecki AA, Pulay P. J. Comput. Chem. 1997; 18:489–500.
87. Davis MI, Orville AM, Neese F, Zaleski JM, Lipscomb JD, Solomon EI. J. Am. Chem. Soc. 2002; 124:602–614. [PubMed: 11804491]

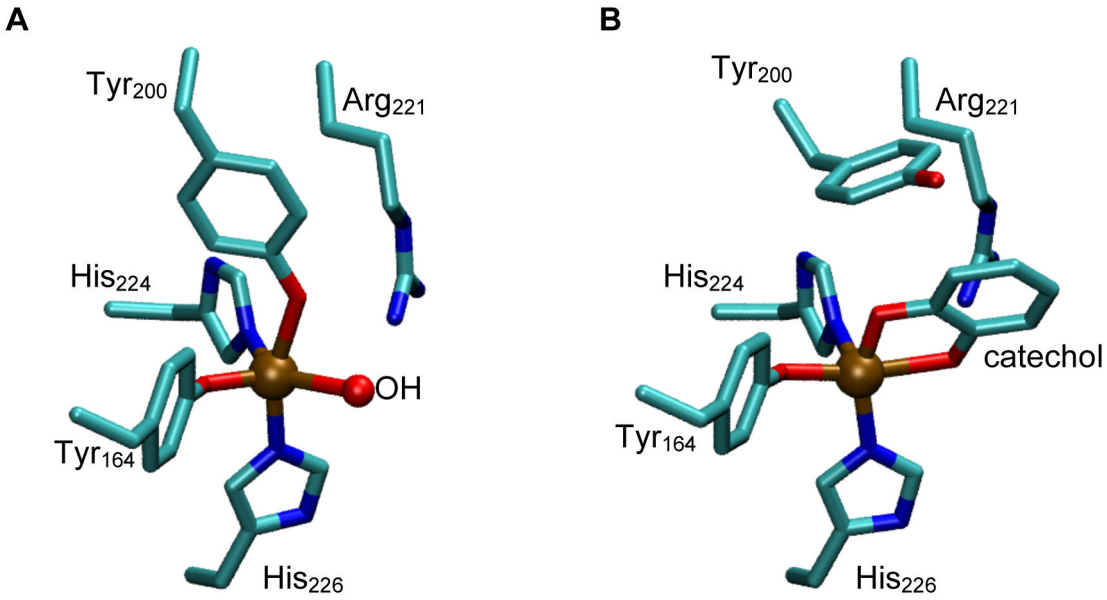

Figure 1.
View of the active site of C12O from *Acinetobacter* sp. ADP1. A) Structure of substrate-free C12O. B) Structure of catechol-bound C12O. Carbon, oxygen, nitrogen, and iron atoms are colored gray, red, blue, and brown, respectively. Arg221 corresponds to Arg218 in the *P. putida* C12O. Arg221 is hydrogen-bonded to the catechol oxygen opposite Tyr164. Adapted from PDB files 1DLM and 1DLT respectively.17 Figure made using VMD.27

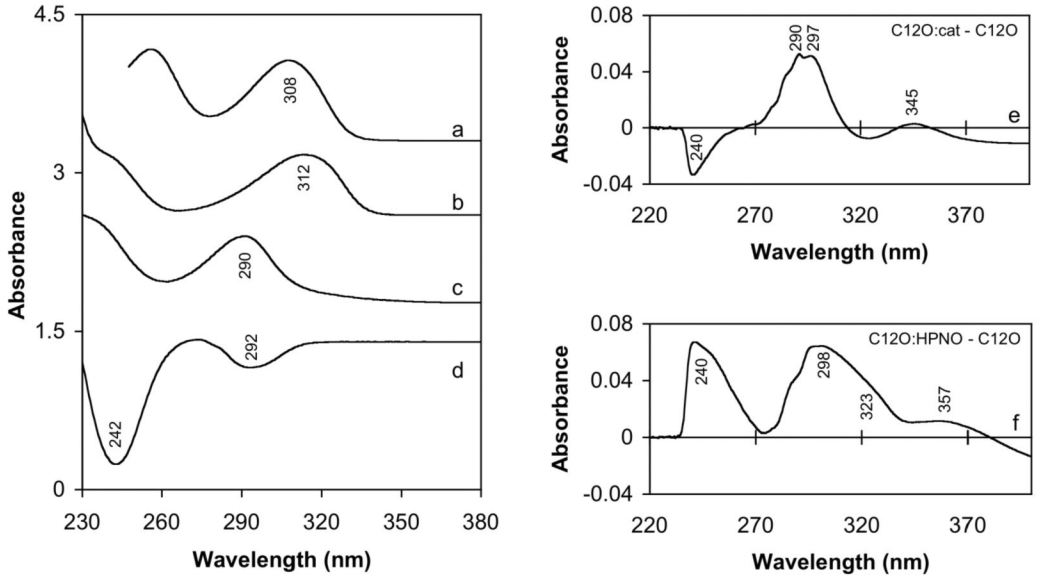

Figure 2.

Electronic absorption spectra of free and enzyme-bound catechol and HPNO compounds. Left panel, spectra of free compounds: (a) Dianionic catechol: 100 μM catechol in 250 mM sodium *tert*-butoxide/*tert*-butanol solution; (b) $HPNO^{-}$: 100 μM HPNO in 20 mM Tris-Cl, 100 mM Na_2SO_4, pH 7.5; (c) Fe(III)-bound dianionic catechol: 32 μM $[Fe(Cat^{2-})_3]^{3-}$ in 0.05% NaOH solution, pH ~12; (d) Difference (tyrosine – tyrosinate) spectrum: [100 μM *N*-acetyl-L-tyrosinamide in potassium phosphate, pH 7 (I = 0.1)] – [100 μM *N*-acetyl-L-tyrosinamide in 0.5% NaOH solution, pH ~13]. For clarity, the spectra have been vertically offset. Right panel, calculated difference spectra for enzyme-bound compounds: (e) C12O:catechol – C12O. Sample contained 20 μM of iron-containing active sites of C12O (93% Fe per homodimer) with 31 μM catechol. (f) C12O:HPNO – C12O. Sample contained 25 μM iron-containing C12O active sites (75% Fe per homodimer) with 24 μM HPNO.

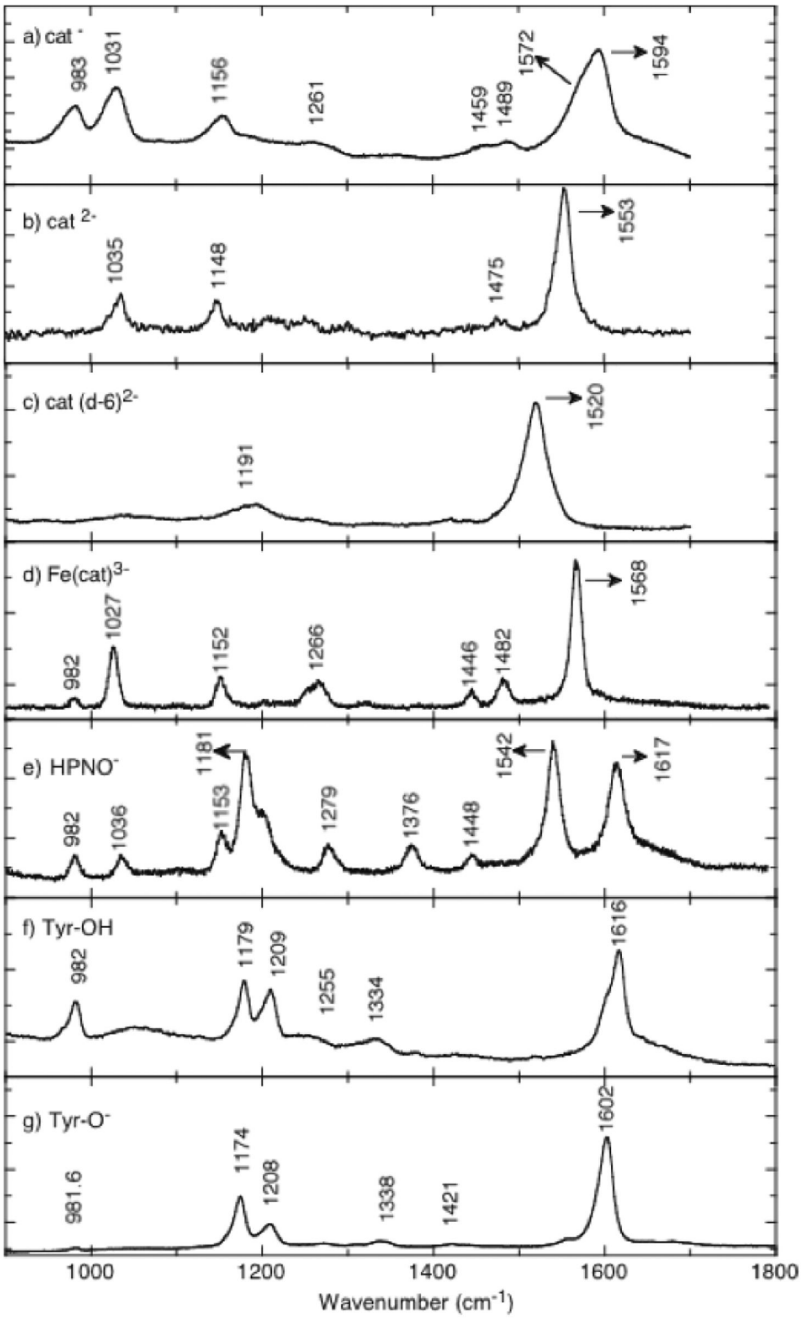

Figure 3.

UVRR spectra of catechol, HPNO, and N-acetyl-L-tyrosinamide. (a) 2 mM catechol in potassium phosphate, pH 11, 100 mM Na_2SO_4 (50 s), (b) 2 mM catechol in sodium *t*-butoxide/*t*–butanol (pH ~18), (180 s), (c) 2 mM catechol-d_6 in sodium *t*-butoxide/*t*–butanol (pH ~18) (~60 s), (d) 2.4 mM $[Fe(Cat^{2-})_3]^{3-}$ in potassium phosphate buffer, pH 11, 100 mM Na_2SO_4, (e) 5 mM HPNO in potassium phosphate buffer, pH 11, 100 mM Na_2SO_4, (f) 10 mM tyrosinamide (tyrosine) in potassium phosphate buffer, pH 7 (I = 0.1), 100 mM Na_2SO_4, (g) 2 mM tyrosinamide (tyrosinate) in 0.5% NaOH solution (~pH 13), 100 mM Na_2SO_4. A comparison of tyrosinamide intensities can be made based on the ~980 cm^{-1} SO_4^{2-} signal, which is present at 100 mM in both spectra. We therefore estimate a 3-fold

greater signal intensity for tyrosinate. Considering the 5-fold concentration difference, tyrosinate provides ~15× more signal than tyrosine. Acquisition times are shown in parentheses.

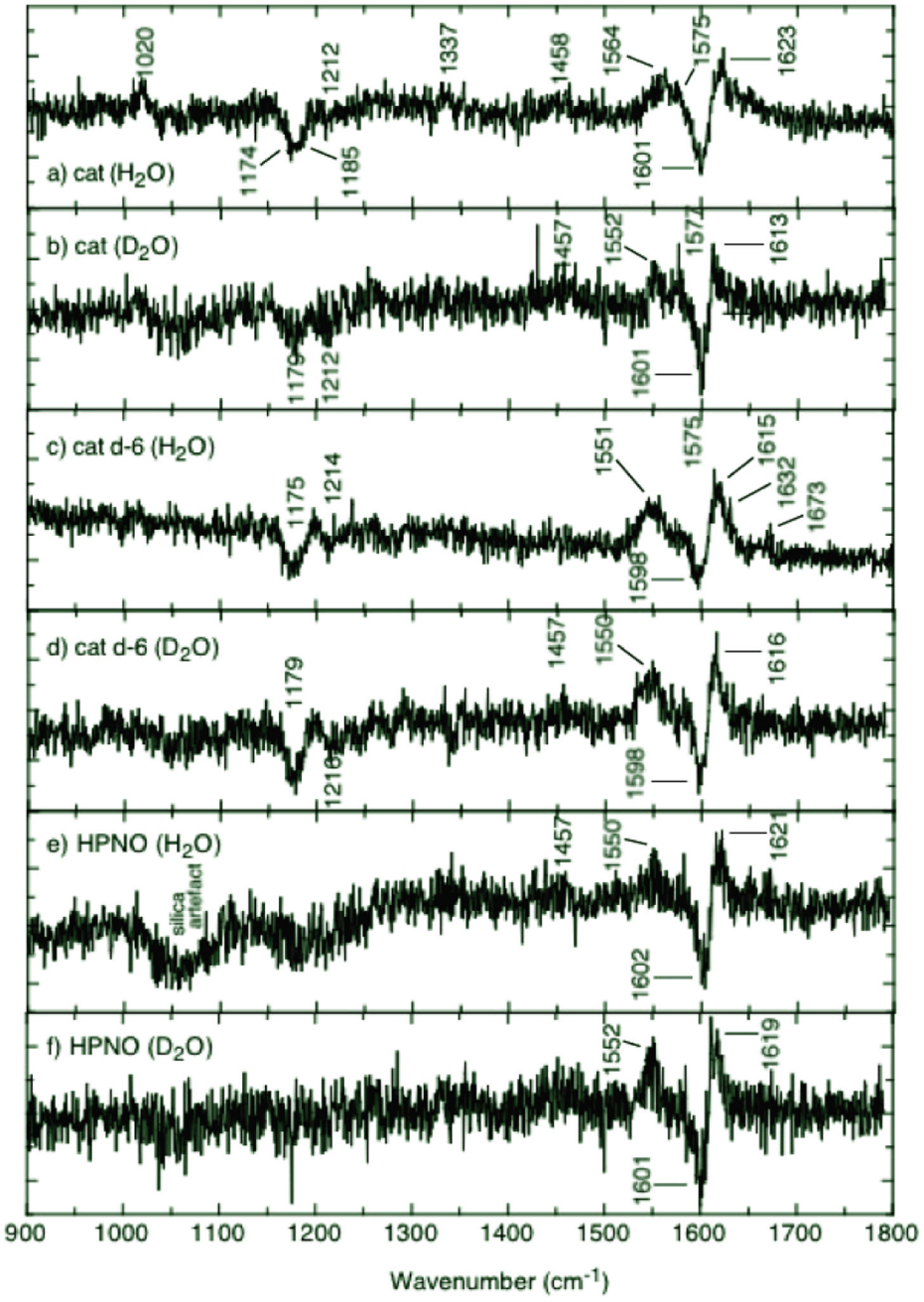

Figure 4.

Difference spectra (ES – E) at pH/pD 7.5 of C12O complexed with catechol or HPNO. (a) C12O and catechol in H_2O; (b) C12O and catechol in D_2O; (c) C12O and catechol-d_6 in H_2O; (d) C12O and catechol-d_6 in D_2O; (e) C12O and HPNO in H_2O; (f) C12O and HPNO in D_2O. Conditions: buffer = 20 mM Tris-Cl, pH/pD 7.5, 100 mM Na_2SO_4; C12O:catechol concentrations = 170:150 μM; C12O:HPNO concentrations = 130:120 μM. C12O concentrations refer to the Fe-containing active sites, and this preparation contained 75% Fe per homodimer.

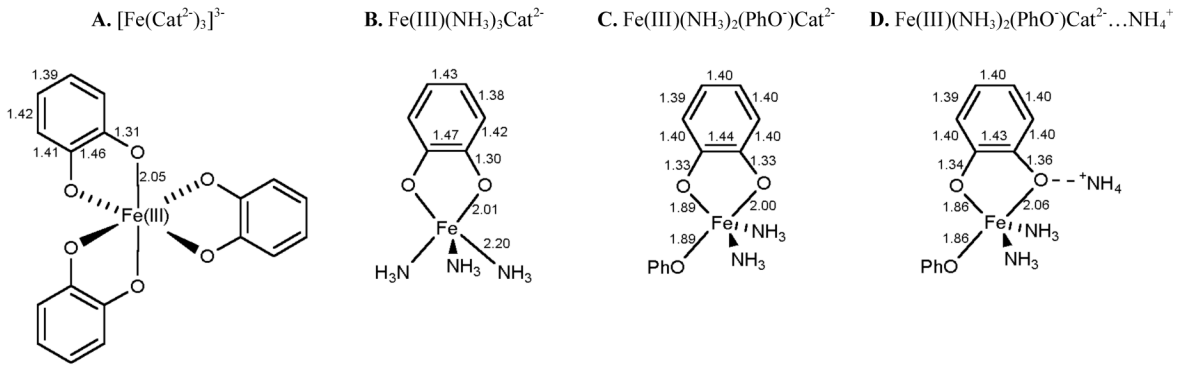

Figure 5.
DFT-computed structures with bond distances in Å.

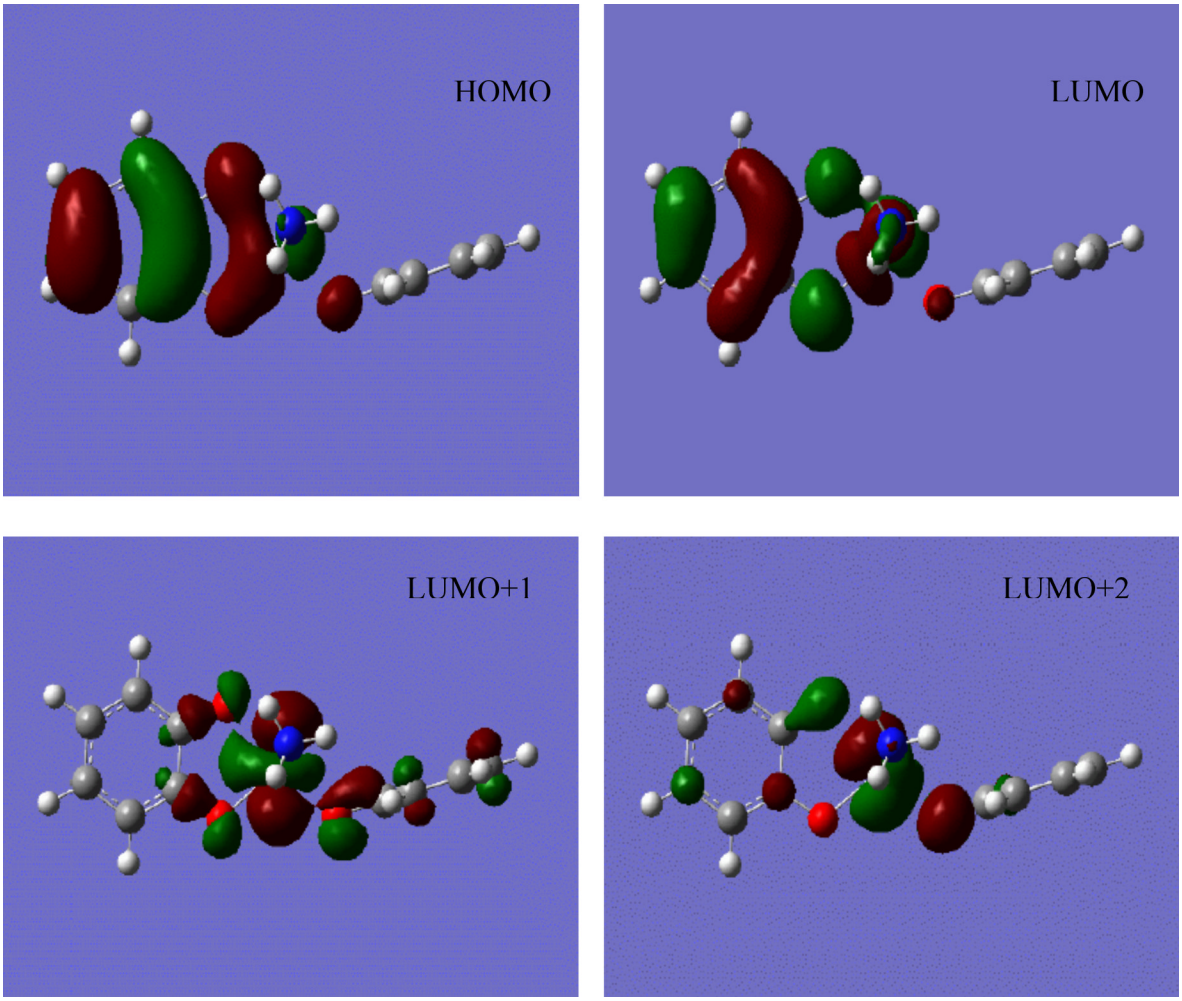

Figure 6.

Frontier orbitals for the Fe(III)$(NH_3)_2(PhO^-)Cat^{2-}$ model (Figure 5C), computed via DFT, extending over the catecholate (left), phenoxide (right) and ammonia ligands (one in front and one hidden in back). The first three excited states, computed via time-dependent DFT, are primarily (>83%) excitations from the HOMO to the LUMO+1 (0.75eV), the LUMO+2 (0.82eV) and the LUMO (1.46eV), respectively. The atoms are shown as white (H), grey (C), red (O) and blue (N) spheres (with Fe buried in the orbital lobe), while the orbital lobes are shown in green and brown (opposite phases).

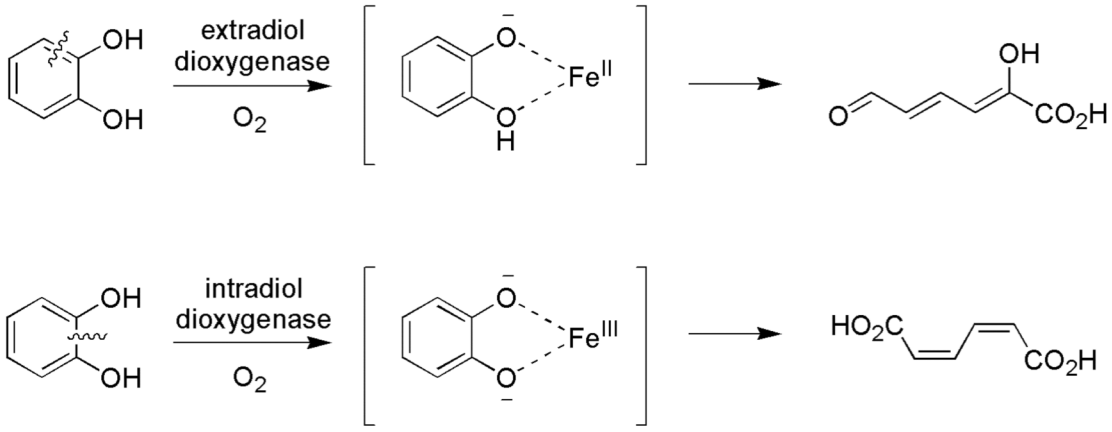

Scheme 1.

Table 1

Band positions for the three ionic forms of catechol (Cat), the $[Fe(Cat^{2-})_3]^{3-}$ model compound ($Fe:Cat^{2-}$), and the enzyme difference spectra (ES – E).

Cat (H)[a]	H:D shift	Cat^{-} (H)	H:D shift	Cat^{2-} (H)	H:D shift	$Fe:Cat^{2-}$ (H)	H:D shift	$Fe:Cat^{2-}$ - Cat^{2-}	ES – E (H)	H:D shift	Assignment[b]
									1623(s)	−2	Tyrosine
									1601(n)	0	Tyrosinate
1599(m)	−2	1594(s)	−6	1553(s)	−1	1568(s)	0	15	1564(s)	−10	νCC A1 (8a)
		1572(m)	−2								νCC B_{3u}
		1489(w)	1	1475(w)	0	1482(m)	1	7			νCC A1 (19b)
1455(w)	0	1459(w)	−2			1446(mw)	0		1459(m)	−2	νCC B2 (19a)
1271(ms)	5	1261(w)	-	1251(w)	1	1266(m)		15			νCO A1 (7a)
									1211(n)	-	Tyrosinate
									1175(n)	2	Tyrosinate
1151(w)	−2	1156(m)	−1	1148(m)	0	1152(m)	−1	4			δCH A1 (9a)
1036(s)	2	1031(s)	2	1035(m)	−2	1027(s)	0	−8	1020(m)	−2	δCH A1 (18b)

Positions and shifts are in wavenumbers.

[a] Band intensity denoted by: s: strong, m: medium, w: weak, n: negative.

[b] Assignments based on comparisons to catechol. Symmetry assignments are based on comparison to catecholate model spectra.[78,82–84]

Table 2

DFT–computed UVRR band positions for the indicated complex and experimental data (Exp) for $[Fe(Cat^{2-})]^{3-}$.

Symmetry	$[Fe(Cat^{2-})_3]^{3-}$	$[Fe(Cat^{2-})_3]^{3-}$			$Fe(III)(NH_3)_3Cat^{2-}$	$Fe(III)(NH_3)_2(PhO^-)Cat^{2-}$	$Fe(III)(NH_3)_2(PhO^-)Cat^{2-}\ldots NH^{4+}$	Wilson number[c]
C_{2v}	Exp	Cal. (D3)	Scaled	d12-shift	Cal. (Cs)	Cal. (Cs)	Cal. (Cs)	
A1	1027[a]	1036	1005	−205	1023	1044	1058	18b
B2		1098	1070	−228	1152	1133	1139	–
A1	1152[a]/1154[b]	1152	1121	−238	1187	1166	1182	9a
B2	1216[b]	1245	1216	−215	1246	1251	1264	-
A1	1266[a]/1262[b]	1330	1288	−72	1337	1276	1287	7a
B2	1322[b]	1349	1311	−70	1375	1325	1308	3
A1	1359[b]	1377	1336	−43	1392	1334	1343	14
B2	1446[a]/1448[b]	1481	1440	−75	1507	1501	1500	19a
A1	1482[a]/1487[b]	1562	1502	−20	1512	1470	1481	19b
B2		1582	1539	−33	1621	1630	1633	8b
A1	1568[a]/1572[b]	1595	1548	−35	1570	1601	1613	8a

[a] Present work

[b] reference 46

[c] reference 77,78,83,84.